LONG-TERM ATMOSPHERIC CORROSION OF MILD STEEL

D. de la Fuente, I. Díaz, J. Simancas, B. Chico and M. Morcillo[*]

National Centre for Metallurgical Research (CENIM-CSIC), Avda. Gregorio del Amo, 8, 28040-Madrid, Spain.

Abstract

A great deal of information is available on the atmospheric corrosion of mild steel in the short, mid and even long term, but studies of the structure and morphology of corrosion layers are less abundant and generally deal with those formed in just a few years. The present study assesses the structure and morphology of corrosion product layers formed on mild steel after 13 years of exposure in five Spanish atmospheres of different types: rural, urban, industrial, and marine (mild and severe). The corrosion layers have been characterised by X-ray diffraction (XRD) and scanning electron microscopy/energy dispersive X-ray spectroscopy (SEM/EDS). Long-term corrosion is seen to be more severe in the industrial and marine atmospheres, and less so in the rural and urban atmospheres. In all cases the corrosion rate is seen to decrease with exposure time, stabilising after the first 4-6 years of exposure. The most relevant aspects to be noted are: (a) the great compaction of the rust layers formed in the rural and urban atmospheres; (b) the formation of hematite and ferrihydrite phases (not commonly found) in the industrial and marine atmospheres, respectively; and (c) identification of the typical morphological structures of lepidocrocite (sandy crystals and flowery plates), goethite (cotton balls structures), and akaganeite (cotton balls structures and cigar-shaped crystals).

Key words: A. Mild steel; B. XRD; B. SEM; C. Long-term atmospheric corrosion; C. Morphology.

1. INTRODUCTION

Steel is the most commonly employed metallic material in open-air structures and is used to make a wide range of equipment and metallic structures due to its low cost and

[*] Corresponding author: Tel. +34 91 553 8900, Fax. +34 91 534 7425. E-mail: morcillo@cenim.csic.es (M. Morcillo)

good mechanical strength. Much of the steel that is manufactured is exposed to outdoor conditions, often in highly polluted atmospheres where corrosion is much more severe than in clean rural environments.

The atmospheric corrosion of mild steel is an extensive topic that has been studied by many authors. Useful reviews have been performed by several researchers [1-5].

A large amount of information is available on the atmospheric corrosion of mild steel in the short and mid term. Information on long-term exposure (10-20 years) is considerably less abundant, and no consistent data is available for exposure times over 50 years [6].

A great deal of effort has been dedicated to identifying corrosion products and quantifying the effect of corrosion in terms of mass loss, and a number of models have been developed to describe the influence of various environmental parameters on the corrosion rate; particularly the sulphur dioxide and chloride concentration [7]. An aspect that has been relatively little studied is the morphology of the corrosion products that grow on the steel surface in the form of thin or thick films.

The present study concentrates on the morphology of corrosion product films formed on mild steel after long-term atmospheric exposure (13 years) in five Spanish atmospheres of different types: rural, urban, industrial, mild marine and severe marine. Characterisation was performed by scanning electron microscopy/energy dispersive X-ray spectroscopy (SEM/EDS), X-ray diffraction (XRD), and extractable ion (SO_4^{2-}, Cl^-) analysis.

2. EXPERIMENTAL

Mild steel test panels, with a composition of (wt.%) 0.44 C, 0.40 Mn, 0.018 S, <0.22 P, <0.05 Si, <0.1 Cr, <0.1 Ni, <0.1 Mo and <0.05 Cu, were exposed at five sites each representing a different type of atmosphere: rural (El Escorial), urban (Madrid), industrial (Bilbao) and marine (Barcelona and Alicante, 30 m from the seashore). Table 1 summarises the environmental characteristics of the test sites.

The rural site of El Escorial is characterised by low sulphur pollution levels and insignificant chloride levels. The surrounding area is mainly forested with some residential (holiday home) areas. The urban atmosphere of the Madrid test site is characterised by moderate SO_2 levels and insignificant chloride levels. The test panels were exposed on the CENIM roof terrace, close to a road with considerable traffic, which accounts for the SO_2 levels encountered. The industrial atmosphere is represented

by the Bilbao test site, located in the industrial setting of a shipyard at Sestao; specifically on the roof terrace of the chemistry laboratories. The atmosphere here is of an acid nature, and Bilbao's climate is characterised by a high number of rainy days and a high annual rainfall rate. These are important factors that need to be taken into account when interpreting the results obtained at this test site. The two marine atmospheres in this study are represented by the Barcelona and Alicante test sites, both located within 30 m of the seashore; the former in the city of Barcelona (urban character) and the latter in an aluminium plant (industrial character). The Alicante test site is characterised by high chloride levels (mainly NaCl) and relatively high sulphur levels (mainly SO_2, Na_2SO_4).

All the sites were equipped with temperature and humidity recorders and the instrumentation necessary to measure atmospheric pollution in terms of SO_2 [10] and Cl^- [11]. The time of wetness was estimated from the number of hours per year that the relative humidity was equal to or above 85% and the temperature exceeded 0ºC.

The panels were exposed in triplicate on open-air racks at an angle of 45º from the horizontal plane. Batches were withdrawn after 1-6, 8, 10 and 13 years of exposure. The corrosion data obtained after 1-6, 8 and 13 years of exposure has been published elsewhere [12-15]. After their final withdrawal, one of the specimens was used to study the composition and morphology of the corrosion products that had formed.

The techniques used to characterise the corrosion products were XRD (for identification of crystalline phases), SEM/EDS (for morphological studies and elemental analysis of the surface and cross-sections of the corrosion product films), and the extraction and quantification of soluble salts. XRD measurements were carried out with a D8 Brukers AXS diffractometer equipped with a Cobalt X-ray tube and a diffracted beam monochromator. The generator settings were 40 kV and 30 mA. XRD data was collected over a 2θ range of 10-80º with a step width of 0.03 º and a counting time of 3 s/step. In this study the program MATCH for phase identification in the rust was employed, making a semi-quantitative analysis by using the relationship I/Ic from the Powder Diffraction Files (PDF) card. For the SEM/EDS studies, use was made of a JEOL JXA-840 electron microscope equipped with a Link System electron microprobe. Analyses were carried out in cross-sections and on the surface of the specimens, considering both the skyward and groundward facing sides. For the extraction and quantification of soluble salts, the specimens were placed (separately) in deaerated distilled water at boiling point for 30 minutes, following the method established by

Mayne [16]. The solutions obtained were subsequently filtered and made up to a constant value for the analysis of chlorides and sulphates. The chlorides present in each filtrate were determined using an Orion 94-17B chloride-selective electrode in combination with an Orion 901 ion analyser. Sulphates were determined by the turbidimetric method, according to ASTM standard D516 [17].

3. RESULTS

3.1 Corrosion versus exposure time

Figure 1 shows the variation in the mild steel corrosion rate with exposure time in the different atmospheres. As can be seen, the corrosion rate falls considerably during the first six years of exposure and subsequently levels out. The sharpest initial drop corresponds to the urban atmosphere of Madrid, where the corrosion rate soon approaches that of the rural atmosphere of El Escorial, which is very low right from the start of exposure.

As a result of the strong attack experienced by the test panels exposed in the severe marine atmosphere of Alicante, only traces of the specimens remained after 13 years of atmospheric exposure. For this reason, mild steel corrosion rate data is only available up to 10 years of exposure.

It is widely accepted that the long-term atmospheric corrosion of steel conforms to an equation of the following type:

$$C = C_I t^b \qquad (1)$$

where C is the metal loss after t years, C_I is that in the first year, and b is an exponent that is usually less than unity. The exponent b is in turn a function of the type of atmosphere where the metal is exposed. By plotting the atmospheric corrosion of steel against the exposure time in log-log coordinates, straight lines of variable slopes are obviously obtained.

To determine how the corrosion data obtained at the test station network fitted equation (1), log-log plots were prepared (Figure 2) showing the variation in mild steel corrosion over the 13 years of exposure in the different atmospheres.

The behaviour in the atmospheres of El Escorial (rural) and Madrid (urban) deviates from that predicted by equation (1). Examples of such deviation from the more common fulfilment of the bilogarithmic law can be found in the literature. Significant

improvement or worsening of the environmental quality of the atmosphere, or very notable changes in the physico-chemical characteristics of the rust layers, can produce significant changes in the value of the exponent b [18].

Zhang et al. [19], in a study carried out in China, found also that the steel atmospheric corrosion process was divided into two steps. A higher corrosion rate in the first step than in the second indicated that the rust layer was becoming more compact.

This anomalous behaviour has only been observed in the two aforementioned Spanish atmospheres, which have low SO_2 levels and are unaffected by any marine influence, while the behaviour of steel in the industrial and marine atmospheres follows the power law shown in equation (1). Thus the question is what environmental conditions promote abnormal behaviour? In a previous publication [20] it was speculated that extremely compact rust layers may be formed, hindering the diffusion of reactants, and there is sufficient literature to consider that compact corrosion products improve the protection afforded by rust layers [21-22]. A comparison of these two Spanish sites with similarly polluted test sites in other countries (where the bilogarithmic law is followed), was also done [23].

3.2. Characteristics of corrosion products formed in the different atmospheres

Table 2 shows the crystalline phases encountered in the corrosion products formed on mild steel in the different atmospheres. XRD analysis were performed on powdered rust samples removed from the specimens or on the specimens themselves. A semi quantitative estimate of each detected phase has been made, expressed as a percentage of the total crystalline products found.

The two phases always present are lepidocrocite (γ-FeOOH) and goethite (α-FeOOH), in this order in terms of content in the rust. Other phases usually present in the steel corrosion products are magnetite (Fe_3O_4) or maghemite (γ-Fe_2O_3), which cannot be differentiated by XRD due to their similar crystalline structure [24]. Their preferential location in the lower strata of the rust layer, close to the base steel, explains why they have not been detected in the powder rust samples obtained from the surface of the highly deteriorated steel specimens in the severe marine atmosphere of Alicante. In this case it was not possible to perform XRD determinations on the steel specimens.

Akaganeite (β-FeOOH) is also found in considerable proportions in marine atmospheres.

It is also interesting to draw attention to the presence of hematite (α-Fe_2O_3) and ferrihydrite ($Fe_5HO_8.4H_2O$) in the atmospheres of Bilbao (industrial) and Barcelona (mild marine), respectively; the latter phase in such a low proportion that it was not quantifiable.

Table 3 shows the soluble sulphate and chloride contents extracted from the adherent and non-adherent fractions of the corrosion layers formed on steel exposed to the different atmospheres. The non-adherent corrosion products were separated from the adherent fraction by means of gentle brushing with a steel wire brush. Due to the severe attack of the specimens exposed in the Alicante test site, located 30 m from the shoreline, which had almost completely disintegrated after 10 years, it was not possible to obtain information on soluble salts in that test site.

It is seen how soluble salts are generally concentrated in the inner strata (adherent fraction) of the rust layers as a consequence of ion migration during the atmospheric corrosion process. A certain logical correspondence is also seen between SO_2 and Cl^- contents in the atmosphere (see table 1) and the total sulphate and chloride contents in the corrosion product layers (see table 3). The highest sulphate contents are found in the corrosion product layers formed in the Bilbao atmosphere, with the highest SO_2 pollution, while the highest chloride contents are found in the corrosion layers formed in the marine atmosphere of Barcelona.

4. DISCUSSION

4.1 Long-term atmospheric corrosion of mild steel. An overview.

4.1.1 Nature of corrosion products

Table 4 shows the corrosion products most frequently found in the corrosion layers formed on mild steel exposed to the atmosphere. The nature of the rust constituents is barely affected by the exposure time; in fact, the same species are always detected at a given site, however long the exposure. The time factor only alters the proportions of the constituents or, at most, determines the appearance or disappearance of intermediate or minor compounds.

Reported rust compositions vary widely as a result of differences in the exposure conditions, identification techniques and data interpretation [25]. Although there is general agreement about the presence of lepidocrocite and goethite in the rust composition, while many authors report the predominance of these species [26] others

assign prevalence to amorphous ferric oxyhydroxide [27] or feroxyhyte (δ-FeOOH) [28].

A number of authors mention magnetite as a second-order constituent [26,27], most often in rust developed in marine atmospheres. When magnetite forms it is usually near the metal substrate, where the lower oxygen availability favours its development [27,29]. Its presence is normally associated with a low protective efficiency of the rust layer formed.

Akaganeite is a typical component of rust developed in marine atmospheres. As shown by Keller [30], it can contain up to 6% chloride and be formed at an early corrosion stage in chloride-containing solutions by hydrolysis of $FeCl_3$ or oxidation of $FeCl_2$ in the presence of iron. Nomura et al. [31] suggested an alternative formation pathway, where OH^- and Cl^- react concurrently with Fe^{3+} complexes to yield lepidocrocite and akaganeite, respectively. On contacting the steel surface, akaganeite is gradually transformed into magnetite, which may be the origin of discrepancies in the relative significance of these two constituents [32].

Antunes et al. [33] in a study carried out in different atmospheres (a humid site located in a tropical forest area, an industrial site and a densely populated urban site) in São Paulo (Brazil) found by XRD the presence of hydrated maghemite (γ-$Fe_2O_3.H_2O$) and hematite (Fe_2O_3), as well as lepidocrocite, goethite, magnetite and akaganeite. Maghemite was found in all sites, however hematite was only observed in the industrial atmosphere of Cubatão.

Water-soluble compounds such as $FeCl_3$ and $FeSO_4$, though expected to be present, are often not detected by EDS. This may be because the amounts in question are so small that they are below the detection limit of the instrument, or because they are obscured by the complexity of the oxide scale after prolonged exposure.

Water-soluble compounds have been analysed by Oesch and Heimgartner [34] in Switzerland using ion chromatography with aqueous extracts from plate specimens. Contamination of the surfaces by ionic species varied greatly between the different test sites. As expected, the highest sulphate and chloride concentrations were found on sheltered specimens. The values obtained only serve to give an idea of the situation at the time when the specimens were withdrawn, since they tend to be strongly dependent on deposition and precipitation conditions in the preceding days and weeks.

It is interesting information to know what phases are present in rust according to the type of atmosphere where mild steel has been exposed for long time periods.

Asami [35] analysed rust on mild steel exposed for 17 years in a rural atmosphere. XRD revealed α-FeOOH as the main constituent, along with γ-FeOOH and β-FeOOH. The origin of β-FeOOH was Cl^- from calcium chloride (rather than marine NaCl) used to melt snow on roads during the winter. Magnetite was not detected, because the X-ray incident angle was fixed at 10º, and the results obtained were just from the surface region of the rust layer. These results do not rule out the existence of magnetite underneath.

Dillmann [6], in ancient ferrous artefacts exposed for very long times (several hundred years) to atmospheres of low aggressivity (rural or semi-industrial, not marine), analysed the composition of rust layers using micro-X-ray diffraction under synchrotron radiation (μXRD) and micro-Raman spectroscopy. μXRD showed that α-FeOOH was present in greater proportions (inner layers) than γ-FeOOH (outer layers). The proportion of magnetite found was 10% while β-FeOOH was less frequent, but it was obviously not possible to identify the amorphous phases. In contrast, micro-Raman spectroscopy detected a poorly crystallised maghemite phase (γ-Fe_2O_3) and ferrihydrite, a hydrated iron(III) oxy-hydroxide. The identification of ferrihydrite was confirmed by X-ray absorption methods under synchrotron radiation.

Kamimura et al. [36] characterised rusts formed on a mild steel exposed for 15 years in an industrial environment using Mössbauer spectroscopy and XRD. They reported that the rust formed consisted of crystalline phases (α and γ-FeOOH) and an amorphous-like phase, $Fe_{3-x}O_4$ (γ-Fe_2O_3), that exceeded 50% of the total amount of rust. This amorphous phase was present both in the inner and the outer rust layer.

Oh et al. [37] analysed rust on mild steel exposed for 16 years in an industrial atmosphere using XRD, Raman spectroscopy and Mössbauer spectroscopy. XRD identified the crystalline phases as α-FeOOH and γ-FeOOH, and Raman spectroscopy confirmed the presence of both and identified γ-Fe_2O_3 and Fe_3O_4, while Mössbauer allowed a finer characterisation detecting α-FeOOH (magnetic and superparamagnetic with different phase sizes), γ-FeOOH and γ-Fe_2O_3.

Cook [24], with mild steel exposed for 16 years at rural and industrial sites, showed that a decrease in the amount of nanophase goethite was responsible for increased porosity and time-of-wetness on the steel surface. This in turn led to the formation of maghemite in the less-aerobic environment close to the steel.

Yamashita et al. [38] reported the influence of airborne salt in marine atmospheres on the rust structure, pointing to an increase in the β-FeOOH content and rust particle size

with an increase in the airborne salt level. Magnetite was also found, although the atmospheric salinity was low.

Oh et al. [37] analysed rusts formed on mild steel exposed for 16 years to a moderate marine atmosphere. Using XRD they found goethite, lepidocrocite, maghemite or magnetite, and akaganeite (possible). Raman spectroscopy ruled out the presence of akaganeite and revealed the existence of both maghemite (<5%) and magnetite (<1%). Finally, using Mössbauer spectroscopy they performed a finer identification, revealing and quantifying the presence of magnetic and superparamagnetic goethite (of different sizes) and superparamagnetic maghemite.

Asami [39] also analysed rusts formed on mild steel exposed for 17 years to a coastal industrial atmosphere. The distribution and abundance of α-FeOOH, β-FeOOH, γ-FeOOH, amorphous rust and magnetite in the rust layer were also investigated using transmission electron microscopy (TEM) and electron diffraction (ED). They found that the magnetite concentration was negatively correlated with the akaganeite concentration.

The main constituent was α-FeOOH on both the skyward and groundward facing surfaces, along with β-FeOOH and γ-FeOOH. The specimens contained a large amount of β-FeOOH on the skyward surface. Magnetite was not detected on either surface. These XRD results were just for the surface region of the rust layer, and thus do not rule out the possible existence of magnetite underneath. The deeper region of the rust layer probably contained different species to those observed by XRD for the surface region. Magnetite appeared more on the groundward side than on the skyward side, while γ-FeOOH was more abundant on the skyward side (TEM/ED determinations). No special tendency was seen regarding the abundance of β-FeOOH, in contrast to XRD results for the rust surface layer. It should be remembered that TEM/ED cross section measurements can cover the entire thickness of the rust layer rather than just the surface region.

Siddique et al. [40] studied the rusting of mild steel in a simulated acid rain environment using transmission Mössbauer spectroscopy, identifying the main corrosion products as α-FeOOH, γ-FeOOH and amorphous-like substances, together with a small amount of γ-Fe_2O_3 (6-8%). Kumar et al. [41], using Mössbauer spectroscopy, studied a mild steel exposed to artificial environments with SO_2 and SO_2 + HCl and found that the non-stoichiometry $Fe_{3-x}O_4$ varied both with the environment

and between the internal and external corrosion products, concluding that the non-stoichiometry $Fe_{3-x}O_4$ was an important factor in its corrosion protective ability.

With regard to the relation between the corrosion rate and corrosion products formed on mild steels exposed to the atmosphere, Morales [42] reported an increase in the relative magnetite content for higher corrosion rates in long-term atmospheric corrosion. Cook [24] noted that large particles of goethite and magnetic maghemite were a possible cause of increases in the corrosion rate of mild steel exposed at marine sites. Yasmashita et al. [43] showed a nearly linear relationship between corrosion loss and mass % of β-FeOOH.

The steel corrosion rate in any environment depends on the composition of the rust layer, which can contain α-FeOOH, β-FeOOH, γ-FeOOH, magnetite and amorphous rust, and especially on the α/γ ratio, where α is the mass fraction of α-FeOOH or the sum of α-FeOOH and amorphous rust, and γ is the sum of the mass fractions of γ-FeOOH, β-FeOOH and magnetite [44,45].

4.1.2. Microstructure of corrosion products

Recognition of the structure (morphology) of the rust layer has not commonly performed in atmospheric corrosion studies.

For most iron corrosion products there is more than one possible preparatory method or formation mechanism and the crystal morphology depends on these formation conditions [46], so a wide range of crystal morphologies and crystal sizes are displayed by most iron corrosion products.

Thus, frequently there is a considerable confusion between the different researches at the time to assign a determined morphology to a particular corrosion product.

Rust morphology characterisation has traditionally been performed using techniques such as optical microscopy, polarised light microscopy, SEM, and electron probe micro-analysis (EPMA). However, new techniques that have recently started to be used include transmission electron microscopy (TEM) and electron diffraction (ED), and micro-Raman spectrometry.

According to Fonseca et al. [47], it is strange that although SEM is very useful to show morphology, and is widely used in materials science, it has not until relatively recently become a common technique in atmospheric corrosion studies. Backscattered electron imaging (BSE) in the SEM has successfully been used to study the microstructure of corrosion layers. Moreover, the sensitivity of the backscattered signal to small

differences in the average atomic number makes it possible to know the distribution of sulphur and chloride compounds in the corrosion layers [48].

4.1.2.1 Surface morphology

The surface morphology can vary considerably between different exposure sites. The morphology of the oxide layer formed on mild steels has been observed by a number of authors [33,49-53]. The phases most frequently found present typical structures, for instance: lepidocrocite appears as small crystalline globules (sandy crystals) or as fine plates (flowery structures) (Fig. 3a); goethite appears as globular structures known as cotton balls (semi crystalline goethite) (Fig. 3b) or even as acicular structures (crystalline goethite); akaganeite appears with cotton ball and rosette morphologies [54,55] (Fig. 3c); and δ-FeOOH shows a distorted plate-like morphology [55]. Magnetite comes out as dark flat regions, with circular discs that are more difficult to find.

Rust layers usually present considerable porosity, spallation and cracking (Figure 4). Figure 4a shows an irregular, cracked and non-protective oxide layer (open structure) which allows the easy access of corrosive species to the metallic substrate; the typical situation in atmospheres of high aggressivity. In contrast, compact oxide layers (closed structures) favour the protection of the metallic substrate. The greater the corrosivity of the atmosphere, the easier it is to find very open structures where flaking (Fig. 4b) can occur. The higher the chloride deposition rate in marine atmospheres, the greater the degree of flaking observed; loosely adherent flaky rust favours rust film breakdown (detachment, spallation) and the initiation of fresh attack. The rust layer on the skyward side of the panels is usually thinner and finer than on the rougher groundward side. This roughness is due to the large rust particles and easy spallation of large flaky rust [34]. Figure 4c shows an example of porosity of a rust layer.

4.1.2.2 Cross-section morphology

The use of complementary analytical techniques, such as X-ray micro diffraction (μXRD), X-ray absorption under synchrotron radiation, Mössbauer spectroscopy, SEM/EDS, TEM/ED, Raman spectroscopy, etc., has allowed a more precise description of the organisation of the corrosion product layer and thus a better understanding of the corrosion layers formed after long-term exposure in air.

Stratification of the rust layer

There is controversy about the stratification of the rust layer in different sublayers [25], as occurs in the case of weathering steels. Suzuki [556] notes that the rust layer formed on unalloyed steel generally consists of two regions: an inner region, next to the steel/rust interface, often consisting primarily of dense amorphous FeOOH with some crystalline Fe_3O_4; and an outer region consisting of loose crystalline α-FeOOH and γ-FeOOH. However, Okada et al. [57] report the inexistence of a dual-layer structure on mild steel exposed to atmospheric corrosion.

Most researchers endorse the concept of the dual-nature rust layer with some or other predominant constituents; in any case, the occurrence of a heavier, more adherent inner sublayer that affords protection and a weaker, more permeable outer sublayer, are supported for both mild steel and weathering steel.

Asami [39] studied in detail the distribution of corrosion products and elements in the rust layer on mild steel by XRD and EPMA, and reported that the rust layer frequently consists of three layers: the inner layer, outer layer and an outermost layer. This external sublayer can accumulate exogenous substances present in the atmosphere, such as chlorides, silica and alumina, originating from sea aerosols and atmospheric deposits of soils, sand, dust, etc.

Distribution of corrosion products inside the corrosion layers

Kamimura et al. [36] characterised rusts formed on mild steel exposed for 15 years in an industrial environment using Mössbauer spectroscopy and X-ray diffraction (XRD). They reported that the rust consisted of crystalline α-FeOOH, γ-FeOOH, and an amorphous-like phase, and that the amount of the amorphous-like phase exceeded 50% of the total rust. Mössbauer spectra indicated that the rust contained only α-FeOOH, γ-FeOOH and $Fe_{3-x}O_4$ (γ-Fe_2O_3). The amorphous-like substance in the rust layer formed on mild steel possessed the structures of mainly α-FeOOH, showing superparamagnetism owing to its small particle size, and $Fe_{3-x}O_4$ (γ-Fe_2O_3), which were contained both in the inner and the outer rust layers.

The cross section of the rust layer is wavy and undulating, with thick and thin parts (Fig. 5). Thus the thickness of the rust layer is quite uneven. According to Asami and Kikuchi [35], there can be no argument that the origin of unevenness comes from the non-uniform distribution of physical and chemical factors, such as environmental deposits and the direction of crystallites in the steel. The thin parts of the rust layer correspond to regions where a protective rust layer covers the steel, whereas the rust

layer in the thick parts is less protective. Asami and Kikuchi [35], in an interesting work on mild steel specimens exposed for 17 years under a bridge in a coastal industrial atmosphere, focus on differences between the composition of the thick and thin parts of the rust layer. Using TEM/ED they try to determine the proportion (semi-quantitative) of α-FeOOH, β-FeOOH, γ-FeOOH, Fe_3O_4 and amorphous rust in the rust layer cross section, as identified by ED patterns. As this technique cannot distinguish between maghemite (γ-Fe_2O_3) and magnetite, the contribution of both was assigned to magnetite.
The main rust constituent was α-FeOOH, which appeared almost homogenously throughout the rust layer. The chief difference between the thick and thin parts was the β-FeOOH and magnetite concentration; there being more β-FeOOH and less magnetite in the thick part of the rust layer. The formation of magnetite (or $Fe_{3-x}O_4$) and β-FeOOH is competitive, i.e. β-FeOOH is preferentially formed when there are chloride ions. The average magnetite concentration in the rust layer is negatively correlated with the β-FeOOH concentration. Akaganeite (β-FeOOH) is generally distributed in the surface region of the rust layer, probably due to the reaction between iron ions produced by corrosion and deposited atmospheric Cl^- ions. This species also appears in the inner layer due to Cl^- ions accidentally entering this region as water deposits containing chloride ions penetrate through cracks in the rust layer.
On the other hand, the thin rust part, where the main constituent is α-FeOOH and the β-FeOOH concentration is very low, has a protective nature because of the stabilised α-FeOOH and it is difficult for chloride ions to enter the rust layer.
The γ-FeOOH concentration and distribution bore no apparent relation with the type of steel, side of exposure or rust thickness. According to Yamashita et al. [44], γ-FeOOH should exist on top of the α-FeOOH rust layer. However, it is not necessarily located in the upper part of the rust layer.
The location of amorphous rust is clear: near the boundary between the rust layer and the steel surface. Its concentration does not bear any relation with the thickness or the type of steel, but its quantification is difficult with the usual analytical techniques.
Dillmann et al. [6], in a study of ancient rusts (hundreds of years old) using optical microscopy, observed the existence in cross sections of a lighter component forming veins in small areas (Fig. 6) inside the corrosion scale, which he identified as ferrihydrite by X-ray absorption under synchrotron radiation. This phase is less crystallised and frequently designated as amorphous rust or a hydrated iron(III) oxyhydroxide.

Dillmann [6], using a wide range of classic and advanced techniques (μXRD, small angle X-ray scattering (SAXS), etc.), studied the composition, structure and porosity of ancient corrosion layers, finding:

(a) the main crystallised phases were Fe_3O_4, α-FeOOH and γ-FeOOH

(b) α-FeOOH has a fairly uniform distribution, occupying most of the rust layer thickness and was in contact with the base metal.

(c) although presenting the same optical appearance as goethite, γ-FeOOH was always confined to small zones in the outer part of the corrosion scale, often located along cracks.

(d) β-FeOOH is located in the outer part of the corrosion layer, sometimes along cracks. Akaganeite is also detected in the inner part of the corrosion products.

(e) lighter veins or areas observed under the optical microscope correspond to the hydrated iron oxyhydroxide (ferrihydrite).

(f) No amorphous phases were clearly identified. This seems to be in contradiction with some authors, who have often found amorphous phases in the inner rust layer. According to Dillmann [6], the old age of the rust could explain the apparent absence of amorphous phases. This hypothesis is also proposed by Yamashita [44], who suggests that during long exposure the amorphous inner layer may be transformed into a densely packed aggregate of goethite nanoparticles.

One of the latest advances in knowledge of the composition of rust layers formed during long-term exposure in the atmosphere is due to Oh et al. [37]. According to these researchers, the inner layer consists of interdispersed goethite in large fractions and superparamagnetic maghemite in small fractions, and the outer layer is composed of interdispersed goethite in small fractions and lepidocrocite in large fractions, irrespective of the environment and the type of steel.

Defects in the rust layer

In atmospheric exposure, wetting and drying cycles influence the structure of the rust layer and its protective properties. Rust formed on steel freely exposed to rain shows a dense (less porous) and laminated structure, compared to the less protective powder-like grainy structure of the rust formed on sheltered surfaces [58] where diffusion to the steel/rust interface is less impeded.

The interior of rust layers exhibit a large number of pores (voids) and microcracks that make them highly defective and permeable to further attack (Figure 7). As time elapses,

the number and size of defects may decrease due to compaction, agglomeration, etc. of the rust layer, thereby lowering the corrosion rate. Almeida et al. [59,60] reported that the rust layers formed during atmospheric exposure grow and become more compact with exposure time, increasing their protectiveness, as was confirmed by a decreasing corrosion rate.

Dillmann [6], in his study with ancient rusts, pointed out that a number of cracks were observed in the rust. These cracks, sometimes of a magnitude of several hundreds of micrometers, could be either perpendicular or parallel to the layers. Neverthless, despite the presence of cracks the rust layers were relatively dense and adherent.

4.1.3 Prediction of corrosion rates

Mass loss measurements for mild steel in long-term exposure to different types of atmospheres show that the steel continues to corrode throughout the exposure time, irrespective of the test site location. The corrosion layers that form on mild steel are generally not very adherent or protective against further corrosion. This commonly results in the build-up of sheets of thick rust as the steel continues to corrode. The sheets eventually become detached and the exfoliated rust again exposes the steel to the atmosphere [24].

It is widely accepted that long-term atmospheric corrosion of steel conforms to an equation of the form:

$$C = at^b \tag{1}$$

where C is the metal loss, t is the exposure time in years, and a and b are constants. According to Benarie and Lipfert [61], equation (1) is a mass-balance equation showing that the diffusional process is rate-determining, and this rate depends on the diffusive properties of the layer separating the reactants.

The accuracy of equation (1) and its reliability to predict long-term corrosion have been demonstrated by Bohnenkamp et al. [20], Legault and Preban [62], Pourbaix [63], Feliu and Morcillo [12], and Benarie and Lipfert [61], among others.

The exponential law, equation (1), with b close to 0.5, can result from an ideal diffusion-controlled mechanism when all the corrosion products remain on the metal surface. This situation seems to occur in slightly polluted inland atmospheres. On the other hand, b values of more than 0.5 arise due to acceleration of the diffusion process

(e.g. as a result of rust detachment by erosion, dissolution, flaking, cracking, etc.). This situation is typical of marine atmospheres, even those with low chloride contents. Conversely, b values of less than 0.5 result from a decrease in the diffusion coefficient with time through recrystallisation, agglomeration, compaction, etc. of the rust layer.

In the special case when b = 1, the mean corrosion rate for one-year exposure is equal to a, the intersection of the line on the bilogarithmic plot with the abscissa t = 1 year. There is no physical sense in b > 1, as b = 1 is the limit for unimpeded diffusion (high permeable corrosion products or no layer at all). Values of b > 1 occur practically as exceptions, due to outliers in the weight loss determinations, for example. As a rule, b < 1.

Therefore, b could be used as an indicator for the physico-chemical behaviour of the corrosion layer and hence for its interactions with the atmospheric environment. The value of b would thus depend both on the metal concerned, the local atmosphere, and the exposure conditions.

On the basis of equation (1), Townsend and Zoccola [64] use as an indicator of the atmospheric corrosion of different steels the time to exhibit a loss of 250 μm calculated by solving equation (2) for time:

$$t^* = [C^*/a]^{1/b} \qquad (2)$$

where:

t* = time in years to achieve a 250 μm corrosion loss;

C* = selected corrosion loss (250 μm), and

a and b = constants of equation (1).

Some authors [65-67], however, use a mixed linear-exponential equation, according to which a plot of corrosion against time would consist of an initial parabolic portion followed by a straight line. McCuen and Albrecht [67] compared both models on the basis of atmospheric corrosion data for weathering steels reported in the United States, concluding that the experimental data fitted the power-linear model better than the power model. This suggests that the former provides more accurate predictions of long-term atmospheric corrosion.

The authors [15] studied the goodness of the power model (Eq. 1) on the basis of all the information compiled for mild steel in a comprehensive literature survey of corrosion

data obtained for exposures of 10 years or more. It was decided to use this model rather than the power-linear model on account of its greater simplicity. In fact, only exponent b and corrosion after the first year of exposure, a, need to be known. The primary aim of that work was to determine b in terms of the type of atmosphere concerned.

As a conclusion of that study, the test stations were grouped according to the local atmosphere type. Rural-urban atmospheres and industrial atmospheres, without any marine component, were distinguished from marine atmospheres. While exponent b varied greatly within each group, a trend was observed in these long-term tests for slopes of between 0.3 and 0.7 for rural, urban and industrial atmospheres and significantly greater (0.6-0.9) for marine atmospheres, whether or not they were close to the shoreline. This confirms the high significance of the marine atmosphere variable (which does not distinguish between chloride levels but refers exclusively to the marine character) in exponent b, as observed in a statistical study [68]. The lower b is, the more protective the corrosion product layer on the metal surface.

Dean [69] reviewed the results obtained for steel in 8-year data from the ISOCORRAG collaborative programme [70]. The time of wetness (TOW) affected positively the value of b for steel, i.e. a higher TOW causes the rust layer to be less protective. The other environmental effects (SO_2 and Cl^-) do not appear to be significant in affecting the slope. However, sulphation and salinity strongly affected the intercept (log a).

With regard to skyward-groundward values for steel, exponent b is higher on the groundward side, demonstrating the higher porosity there [61].

4.2. Long-term atmospheric corrosion in Spain

4.2.1 Rural (El Escorial) and urban (Madrid) atmospheres

The corrosion of mild steel in these atmospheres is relatively low (Table 1), especially in the case of the rural atmosphere, where corrosion in the first year is only 7.5 μm. The corrosivity category is in the interval C2 (low) - C3 (medium), according to ISO 9223 [9]. After 13 years of atmospheric exposure, the attack of the base steel is fairly regular and the rust layers have a thickness of between 100 and 200 μm.

The corrosion rate decreases with exposure time (Fig. 1), giving rise to great compaction of the rust layer (Fig. 8), so that after 4-6 years of atmospheric exposure a strong change takes place in the kinetics of the atmospheric corrosion process (Fig. 2).

The behaviour in the Spanish atmospheres of El Escorial (rural) and Madrid (urban) deviates from that predicted by equation (1). The log-log plot of steel corrosion vs. time

for these two atmospheres (Figure 2) is a broken line consisting of two linear segments: an initial segment with a slope of 0.73 (El Escorial) or 0.48 (Madrid) followed by a second segment with a very gentle slope (0.08 and 0.09, respectively) [20]. Looking for the main cause of this anomalous behaviour, in a comparison of these two Spanish sites with test sites in other countries (where the bilogarithmic law is followed), such as the former Czechoslovakia [23], with similar annual precipitation and atmospheric pollution by SO_2 and chlorides, it was concluded that the higher relative humidities and time-of-wetness at the Czech sites must favour the formation of loose, non-compact oxide. On the other hand, the longer annual hours of sunlight and higher air temperature of the Spanish sites results in shorter drying times and hence in the formation of more compact rust layers [20].

The corrosion products formed in these atmospheres, identified by XRD (Table 2), were: lepidocrocite (γ-FeOOH) (60.6%), goethite (α-FeOOH) (24.6%) and magnetite (Fe_3O_4)/maghemite (γ-Fe_2O_3) (14.8%). As has been noted above, XRD cannot differentiate between the latter two compounds. Typical lepidocrocite formations, in the form of flowery structures, and goethite formations, in the form of cotton balls, can be observed in Figure 9.

With regard to the soluble salts content in the corrosion layers formed (Table 3), this is lower than in the other atmospheres, and in consonance with the low atmospheric SO_2 and Cl^- levels (Table 1), as can also be seen in the EDS spectrum obtained for the rust layer formed in the Madrid atmosphere after 13 years of exposure (Fig. 8).

Figure 10 shows SEM views of the surface of the rust layers formed on the skyward and groundward sides, respectively, after 13 years of exposure in the El Escorial atmosphere. Together with the micrographs, the EDS spectra show the presence exogenous elements present in the atmosphere, such as silica, alumina, calcium and potassium, originating from the land in the test site area. The longer times of wetness of the groundward surfaces and the absence of any washing effect due to the action of the rain, removing the deposited saline pollutants, means that the corrosion product layers formed (Fig. 10, right) exhibit more open structures and thus with fewer protective properties than those formed on the skyward surface (Fig. 10, left).

4.2.2 Industrial atmosphere (Bilbao)

Steel corrosion is considerable in the industrial atmosphere of Bilbao, with high SO_2 pollution (corrosivity category C4 (high), according to ISO 9223 [9]), Table 1, and its

evolution with exposure time follows the bilogarithmic law (Eq. (1)), as can be seen in Fig. 2. During the first years of exposure the corrosion product layers become increasingly compact, buffering the corrosion rate which stabilises after 4-6 years (Fig. 1); although cracking continues to be considerable, unlike in the rural and urban atmospheres (Fig. 11). The attack profile of the base steel is also more irregular, with rust layer thicknesses of between 100 and 200 μm.

The corrosion products formed in this atmosphere (Table 2) were (from the greater to lesser proportion): lepidocrocite (γ-FeOOH) (46.5%), hematite (α-Fe_2O_3) (23.3%), goethite (α-FeOOH) (18.9%), and magnetite (Fe_3O_4)/maghemite (γ-Fe_2O_3) (11.4%). Attention is drawn to the presence of large amounts of hematite, which is not found in the other atmospheres, and is not commonly cited in the literature consulted; in the Brazilian station of Cubatao (industrial atmosphere) Antunes et al. [33] also detected the existence of hematite among the corrosion products of steel. According to Cornell and Schwertmann [61] one of the two common ways of producing hematite crystals in aqueous systems is via ferrihydrite ($Fe_5HO_8.4H_2O$) in weak acid media; hematite grows from ferrihydrite at a temperature of <100ºC at a pH where the solubility product of ferrihydrite is exceeded. The somewhat acid rainwater of the industrial atmosphere of Bilbao may perhaps have favoured this transformation.

With regard to the soluble salts content, the rust layers contain important amounts of chlorides and sulphates (Table 3), in concordance with the high SO_2 and Cl^- contents in the atmosphere, exceeded only by the severe marine atmosphere of Alicante (Table 1).

Figure 12 shows the morphologies commonly found for the surfaces of corrosion layers formed in this atmosphere, with formations of goethite (Fig. 12a) and lepidocrocite (Fig. 12b), and corrosion product layers eroded by the somewhat acid rainwater (drizzle) that is common in this industrial atmosphere (Fig. 12c).

4.2.3 Marine atmospheres (Barcelona and Alicante)

Mild steel corrosion in marine atmospheres tends to be high. It is normal to find corrosivity categories C4 (high) and C5 (very high), according to ISO 9223 [9], depending on the atmospheric salinity. The aggressivity of the marine atmosphere of Alicante is very severe, due to the high marine aerosol content, and SO_2 from a nearby aluminium plant; in fact, this is a marine-industrial atmosphere (Table 1). The corrosivity is so severe that the 2 mm thickness steel specimens were practically consumed after 13 years of exposure, leaving only traces of the specimen in the form of

rust flakes (Figure 13). The thickness of the corrosion product layers formed in these environments is usually high, between 100 and 300 μm.

In both marine atmospheres the atmospheric corrosion rate is buffered during the first years of exposure, stabilising at a corrosion rate of 30 or 60 μm/year for the atmospheres of Barcelona and Alicante, respectively (Fig. 1). The corrosion data obtained for these two atmospheres is fitted to the power function (Eq. (1)), being straight lines of a similar slope (b = 0.70 and 0.80) in the log-log plots (Fig. 2).

The corrosion products identified by XRD in the Barcelona and Alicante atmospheres were repetitively lepidocrocite (39.1% and 43.2%), akaganeite (35.5% and 39.3%) and goethite (15.8% and 17.5%) (Table 2). Thus there is a preponderance of the first two constituents, which present characteristic morphological structures: sandy crystals (Fig. 14, left), typical of lepidocrocite [33], and cigar-shaped crystals (Fig. 14, right), typical of akaganeite [46]. This structure is not commonly referred in atmospheric corrosion studies of steel.

In the urban-marine atmosphere of Barcelona magnetite/maghemite was also detected (9.6%). As has already been noted, these constituents usually form close to the base steel. It was not possible to detect these phases in Alicante since only surface rust powder, from the milling of the remaining rust flakes, was available for analysis.

Although it was not possible to quantify ferrihydrite ($Fe_5HO_8.4H_2O$), its presence of was also detected on the specimens exposed in Barcelona. Backscattered electron imaging (Fig. 15) indicated the presence of the ferrihydrite phase in the form of veins or isolated regions of a lighter colour tones than the rest of the rust layer [71].

The greater salinity of the marine atmosphere of Barcelona leads to the existence of high soluble chloride concentrations in the corrosion product layers (Table 3). Due to the consumption of most of the specimen exposed in Alicante, it was not possible to determine the soluble salt contents of the specimen.

The SEM/EDS study of the corrosion product layers formed on mild steel in the marine atmospheres showed very open surface morphology structures (Fig. 16) of a low protective power, which do not prevent aggressive environmental agents from reaching the base steel, thus explaining the high steel corrosion rates in these atmospheres.

The cross section of the corrosion product layers formed in these atmospheres show irregular (serrated) attack profiles of the base metal (Fig. 17a), with thin and thick areas in the rust layer. The EDS spectrum of the rust layer shows the presence of exogenous

elements from the marine aerosol (Cl, S, K, Mg) and the land (Si, Al, Ca) where the test rack was located.

The BSE/SEM technique makes it possible to differentiate these elements by their atomic weight, e.g. regions richer in chlorides (dark areas), in the deepest zones of the thick parts of the corrosion product layers close to the base steel (Fig. 17b). The X-ray map of Cl^- (Fig. 17c) and the EDS spectra of the light areas (Fig. 17d) and dark areas (Fig. 17e) confirm the Cl^- enrichment of the latter.

5. CONCLUSIONS

This study of long-term corrosion (13 years) of mild steel exposed to a variety of atmospheres allows the following conclusions to be drawn:

(1) Long-term atmospheric corrosion is low in rural and urban atmospheres but high in industrial and marine atmospheres.

(2) Corrosion data for El Escorial (rural) and Madrid (urban) atmospheres deviate from the common behaviour of fulfilment of the power function (bilogarithmic law): $C=a.t^b$. The great compaction of the rust layers formed in these low pollution atmospheres, due possibly to their special climatology, may have been the cause of this irregular behaviour.

(3) The corrosion products identified by XRD have been: lepidocrocite, goethite, and magnetite/maghemite (in all the atmospheres), akaganeite (only in the marine atmospheres), and hematite (only in the industrial atmosphere of Bilbao). The presence of ferrihydrite is also detected in the marine atmosphere of Barcelona.

(4) The morphological structures found for the corrosion products formed have been the typical sandy crystal (marine atmospheres) and flowery (fine plates) (rest of atmospheres) structures of lepidocrocite; the typical cotton ball structure of goethite; and cotton ball structure and cigar-shaped crystals of akaganeite. Ferrihydrite is observed in the form of veins or light regions in the cross sections of the corrosion product layers.

(5) The morphologies found for the surfaces of the corrosion product layers are usually closed structures on the skyward facing specimen sides in atmospheres of low agressivity. In the rest of the situations studied the structures are open, with less protective power.

(6) The attack profile of the base steel in the marine atmospheres is serrated, with valley regions where chloride ions accumulate.

6. REFERENCES

[1] I.L. Rozenfeld, Atmospheric Corrosion of Metals, NACE, Houston, 1972.

[2] K. Barton, Protection against Atmospheric Corrosion, Wiley, London, 1976.

[3] V. Kucera, E. Mattsson, Atmospheric corrosion, in: F. Mansfeld (Ed.), Corrosion Mechanims, Marcel Dekker, New York, 1987, pp. 211-284.

[4] J.M. Costa, M. Morcillo, S. Feliu, Effect of environmental parameters on atmospheric corrosion of metals, in: P.N. Cheremisinoff (Ed.), Air Pollution Control (Vol. 2), on Encyclopedia of Environmental Control Technology, Gulf Publishing Company, Houston, 1989, pp. 197-238.

[5] C. Leygraf, T.E. Graedel, Atmospheric Corrosion, Wiley – Interscience, New York, 2000.

[6] Ph. Dillmann, F. Mazaudier, S. Hoerlé, Advances in understanding atmospheric corrosion of iron. I. Rust characterisation of ancient ferrous artefacts exposed to indoor atmospheric corrosion, Corros. Sci. 46 (2004) 1401-1429.

[7] S. Feliu, M. Morcillo, S. Feliu Jr., The prediction of atmospheric corrosion from meteorological and pollution parameters—II. Long-term forecasts, Corros. Sci. 34 (1993) 415-422.

[8] M. Morcillo, S. Feliu, Mapas de España de Corrosividad Atmosférica, CYTED, Madrid, 1993.

[9] ISO 9223, Corrosion of Metals and Alloys-Classification of Corrosivity of Atmospheres, ISO, Geneva, 1990.

[10] B.S. 1747: Part. 4, Measurement of Air Pollution, British Standards Institution, London, 1969.

[11] A. Hache, Proc. of the 2nd International Congress on Metallic Corrosion, NACE, New York, 1966, pp. 356.

[12] S. Feliu, M. Morcillo, Atmospheric corrosion testing in Spain, in: W.H. Aylor (Ed.), Atmospheric Corrosion, J. Wiley and Sons, New York, 1982, pp. 913-921.

[13] M. Morcillo, S. Feliu, Datos de corrosión atmosférica en España. Resultados de seis años de exposición, Revista Iberoamericana de Corrosión y Protección XIV, 1983, 89-99.

[14] M. Morcillo, S. Feliu, S. Giménez, Long-term atmospheric corrosion of mild steel, zinc, copper and aluminium in Spain, in: Proc. of the 10th International Congress on Metallic Corrosion, Vol. 1, Oxford and IBH Publishing Co, New Delhi, 1987, pp. 17-33.

[15] M. Morcillo, J. Simancas, S. Feliu, Long-term atmospheric corrosion in Spain: results after 13 to 16 years of exposure and comparison with worldwide data, in: W.W Kirk, H.H. Lawson (Eds.), Atmospheric Corrosion ASTM STP 1239, ASTM Philadelphia, 1995, pp. 195-214.

[16] J.E.O. Mayne, The problem of painting rusty steel, J. Appl. Chem. 9 (1959) 673-680.

[17] ASTM D 516, Standard Test Methods for Sulphate Ion in Water and Waste Water, ASTM, Philadelphia, 1968.

[18] C.R. Shastry, J.J. Friel, H.E. Townsend, Sixteen-year atmospheric corrosion performance of weathering steels in marine, rural and industrial environments, in: S.W. Dean, T.S. Lee (Eds.) Degradation of Metal in the Atmosphere, ASTM STP 965, American Society for Testing and Materials, Philadelphia, 1983, pp. 5-15.

[19] Q.C. Zhang, J.S. Wu, J.J. Wang, W.L. Zheng, J.G. Chen, A.B. Li, Corrosion behavior of weathering steel in marine atmosphere, Mater. Chem. Phys. 77 (2002) 603-608.

[20] M. Morcillo, S. Feliu, J. Simancas, Deviation from bilogarihtmic law for atmospheric corrosion of steel, Br. Corrosion J. 28 (1993) 50-52.

[21] K. Bohnenkamp, G. Burgmann, W. Schwenk, Investigations of the atmospheric corrosion of plain carbon and low alloy steels in industrial, rural and sea air, Stahl Eisen 93 (1973) 1054-1060.

[22] M. Pourbaix, A. Pourbaix, Recent progress in atmospheric corrosion testing, Corrosion 45 (1989) 71-83.

[23] D. Knotkova, P. Holler, State Research Institute for Protection of Materials (SVUOM). Private communication.

[24] D.C. Cook, Spectroscopic identification of protective and non-protective corrosion coatings on steel structures in marine environments, Corros. Sci. 47 (2005) 2550-2570.

[25] C. Arroyave, M. Morcillo, Atmospheric corrosion products in iron and steels, Trends in Corrosion Research 2 (1997) 1-16.

[26] K. Rösler, H. Baum, O. Kukurs, A. Upite, D. Knotkova, Character and behavior of a layer of corrosion products on low-alloy steels in natural conditions, Prot. Met. 17 (1981) 514-522.

[27] T. Misawa, K. Asami, K. Hashimoto, S. Shimodaira, The mechanism of atmospheric rusting and the protective amorphous rust on low alloy steel, Corros. Sci. 14 (1974) 279-289.

[28] A. Raman, B. Kuban, Infrared spectroscopic analysis of phase transformation processes in rust layers formed on weathering steels in bridge spans, Corrosion 44 (1988) 483-488.

[29] R.A. Francis, The morphology of corrosion products on steel, in: Proc. of the 10th International Congress on Metallic Corrosion, Vol. 1, Oxford and IBH Publishing Co, New Delhi, 1987, pp. 121-130.

[30] P. Keller, Occurrence, formation and phase transformation of β-FeOOH in rust, Werkst. Korros. 20 (1969) 102-108.

[31] K. Nomura, M. Tasaka, Y. Ujihira, Conversion electron moessbauer spectrometric study of corrosion products of iron immersed in sodium chloride solution, Corrosion 44 (1988) 131-135.

[32] L. Espada, P. Merino, A. González, A. Sánchez, Atmospheric corrosion in marine environments, in: Proc. of the 10th International Congress on Metallic Corrosion, Vol. 1, Oxford and IBH Publishing Co, New Delhi, 1987, pp. 3-7.

[33] R.A. Antunes, J. Costa, D.L Araujo, Characterization of atmospheric corrosion products formed on steels, Mater. Res. 6 (2003) 403.

[34] S. Oesch, P. Heimgartner, Environmental effects on metallic materials - Results of an outdoor exposure programme running in Switzerland, Mater. Corros. 47 (1996) 425-438.

[35] K. Asami, M. Kikichu, In-depth distribution of rusts on a plain carbon steel and weathering steels exposed to coastal–industrial atmosphere for 17 years, Corros. Sci. 45 (2003) 2671-2688.

[36] T. Kamimura, S. Nasu, T. Tazaki, K. Kuzushita, S. Morimoto, Mössbauer spectroscopic study of rust formed on a weathering steel and a mild steel exposed for a long term in an industrial environment, Mater. Trans. 43 (2002) 694-703.

[37] S.J. Oh, D.C. Cook, H.E. Towsend, Atmospheric corrosion of different steels in marine, rural and industrial environments, Corros. Sci. 41 (1999) 1687-1702.

[38] M. Yamashita, K. Asami, T. Ishikawa, T. Ohtsuka, H. Tamura, T. Misawa, Characterization of rust layer on weathering steel exposed to the atmosphere for 17 years, Zairyo-to-Kankyo 50 (2001) 521-530.

[39] K. Asami, M. Kikuchi, Characterization of rust layers on weathering steels air-exposed for a long period, Mater. Trans. 43 (2002) 2818-2825.

[40] M. Siddique, M. Anwar-ul-Islam, N.M. Butt, N. Hussain, S. Rehman, M. Arshed, Mössbauer study of corrosion of mild steel induced by acid rain, J. Radioanal. Nucl. Chem. 241 (1999) 239-240.

[41] A.V.R. Kumar, R.K. Nigam, S.S. Monga, Bull. Electrochem. 15 (1999) 115

[42] A.L. Morales, D. Cartagena, J.L. Rendon, A. Valencia, The relation between corrosion rate and corrosion products from low carbon steel, Phys. Status Solidi B 220 (2000) 351-356.

[43] M. Yamashita, A. Maeda, H. Uchida, T. Kamimura, H. Miyuki, Crystalline rust compositions and weathering properties of steels exposed in nation-wide atmospheres for 17 years, J. Jpn. I. Met. 65 (2001) 967-971.

[44] M. Yamashita. H. Miyuki, Y. Matsuda, H. Nagano, T. Misawa, The long term growth of the protective rust layer formed on weathering steel by atmospheric corrosion during a quarter of a century, Corros. Sci. 36 (1994) 283-299.

[45] T. Kamimura, M. Yamashita, H. Uchida, H. Miyuki, Correlation between corrosion rate and composition of crystalline corrosion products formed on weathering steels, J. Jpn. I. Met. 65 (2001) 922-928

[46] R.M. Cornell, V. Schwertmann, Iron Oxides in the Laboratory, Wiley-VCH, Weinheim, 1991.

[47] M.P. Cindra Fonseca, I.N. Bastos, A. Caytuero, E.M. Baggio Saitovitch, Rust formed on cannons of XVIII century under two environment conditions, Corros. Sci. 49 (2007) 1949-1962.

[48] J. Simancas, K.L. Scrivener, M. Morcillo, A study of rust morphology, contamination and porosity by backscattered electron imaging, in: W.W Kirk, H.H. Lawson (Eds.), Atmospheric Corrosion ASTM STP 1239, ASTM Philadelphia, 1995, pp. 137-151.

[49] A. Raman, A. Razvan, B. Kuban, K.A. Clement, E. Graves, Characteristics of the rust from weathering steels in Louisiana bridge spans, Corrosion 42 (1986) 447-455.

[50] A. Raman, S. Nasrazadani, L. Sharma, Morphology of rust phases formed on weathering steels in various laboratory corrosion tests, Metalography 22 (1989) 79-96.

[51] A. Raman, S. Nasrazadani, L. Sharma, A. Razvan, Morphology of rust phases formed on weathering steels during outdoor atmospheric exposure in open, bold locations, Prakt. Metallogr-Pr. M. 24 (1987) 577-587.

[52] A. Razvan, A. Raman, Morphology of rust phases formed on naturally weathered weathering steels in bridge spans, Prakt. Metallogr-Pr. M. 23 (1986) 223-236.

[53] A. Raman, S. Nasrazadani, L. Sharma, A. Razvan, Prakt. Metallogr-Pr. M. 24 (1987) 535.

[54] M. Morcillo, E. Almeida, B. Rosales, J. Uruchurtu, M. Marrocos, Corrosión y Protección de Metales en las Atmósferas de Iberoamérica (MICAT), CYTED, Madrid, 1998.

[55] K.K. Sagoe-Crentsil, F.P. Glasser, Constitution of green rust and its significance to the corrosion of steel in Portland cement, Corrosion 49 (1993) 457-463.

[56] I. Suzuki, Y. Hisamatsu, N. Masuko, Nature of atmospheric rust on iron, J. Electrochem. Soc. 127 (1980) 2210-2215.

[57] H. Okada, Y. Osoi, K. Yukawa, H. Naito, Proc. of the 4th International Congress on Metallic Corrosion, Amsterdam, 1969, pp. 392-398.

[58] G.B. Clark, G.K. Berukshtis, Z.I. Ignatova, Proc. of the 3rd International Congress on Metallic Corrosion, Moscow, 1969, pp. 406-412.

[59] E. Almeida, M. Morcillo, B. Rosales, M. Marrocos, Atmospheric corrosion of mild steel Part I - Rural and urban atmospheres, Mater. Corros. 51 (2000) 859-864.

[60] E. Almeida, M. Morcillo, B. Rosales, Atmospheric corrosion of mild steel Part II - Marine atmospheres, Mater. Corros. 51 (2000) 865-874.

[61] M. Benarie, F.L. Lipfert, A general corrosion function in terms of atmospheric pollutant concentrations and rain pH, Atmos. Environ. 20 (1986) 1947-1958.

[62] R.A. Legault, G. Preban, Kinetics of the atmospheric corrosion of low-alloy steels in an industrial environment, Corrosion 31 (1975) 117-122.

[63] M. Pourbaix, The linear bilogarithmic law for atmospheric corrosion, in: W.H. Aylor (Ed.), Atmospheric Corrosion, J. Wiley and Sons, New York, 1982, pp. 107-121.

[64] H.E. Towsend, J.C. Zoccola, Eight-year atmospheric corrosion performance of weathering steel in industrial, rural, and marine environments, in: S.W. Dean, E.C. Rhea (Eds.), Atmospheric Corrosion of Metals, ASTM STP 767, American Society for Testing and Materials, Philadelphia, 1982, pp. 45-69.

[65] Y.N. Mikhailovski, et al, Zaschita Metallov, 16 (1980) 396-413.

[66] P. Holler, D. Knotkova, Determination of the corrosivity of atmosphere. Methods and results, Internal Report, State Research Institute for Protection of Materials (SVUOM), Czechoslovakia.

[67] R.H. Mc Cuen, P. Albrecht, Composite modeling of atmospheric corrosion penetration data, in: G. Cragnolino, N. Sridhar (Eds.), Application of Accelerated Corrosion Tests to Service Life Prediction of Materials, ASTM STP 1194, American Society for Testing and Materials, Philadelphia, 1993, pp. 65-101.

[68] S. Feliu, M. Morcillo, S. Feliu, Jr., The prediction of atmospheric corrosion from meteorological and pollution parameters—II. Long-term forecasts, Corros. Sci. 34 (1993) 415-422.

[69] S.W. Dean, D.B. Reiser, Analysis of long-term atmospheric corrosion results from ISOCORRAG Program, in: H.E. Towsend (Ed.), Outdoor Atmospheric Corrosion, ASTM STP 1421, American Society for Testing and Materials, Philadelphia, 2002, pp. 3-18.

[70] S. W. Dean, D. Knotkova, K. Kreislova, ISOCORRAG. International Atmospheric Exposure Program: Summary of Results, ASTM Data Series 71. ASTM International, West Conshohocken, 2010.

[71] D. Neff, L. Bellot-Gurlet, Ph. Dillmann, S. Reguer, L. Legrand, Raman imaging of ancient rust scales on archaeological iron artefacts for long-term atmospheric corrosion mechanisms study, J. Raman Spectrosc. 37 (2006) 1228-1237.

FIGURE CAPTIONS

Figure 1. Variation of mild steel corrosion rate with exposure time at different atmospheric test sites: El Escorial (Rural), Madrid (Urban), Bilbao (Industrial), Barcelona (Mild marine) and Alicante (severe marine).
Each point is a mean value of three specimens. Standard deviation: ±10%

Figure 2. Log-log plots (and the corresponding slopes (n)) of corrosion of mild steel versus exposure time for different atmospheric test sites.

Figure 3. SEM micrographs showing: a) fine plates ("flowery" structures) typical of lepidocrocite, b) globular ("cotton balls") structures typical of goethite, and c) "cotton balls" and "rosette" morphologies typical of akaganeite [70].

Figure 4. SEM micrographs showing: a) cracking, b) flaking and c) porosity of atmospheric corrosion layers formed on mild steel.

Figure 5. Cross section of a rust layer formed on mild steel in a marine atmosphere, showing the presence of thick and thin parts.

Figure 6. Cross section backscattered electron image of a corrosion product layer formed on mild steel in long-term exposure to the atmosphere, showing its mottled structure and a lighter component (ferrihydrite) that forms small areas inside the corrosion scale.

Figure 7. Cross section backscattered electron image of a corrosion layer formed on mild steel in long-term exposure to the atmosphere, showing the presence of pores (voids) and cracks running in perpendicular and parallel directions.

Figure 8. Cross section SEM micrographs of corrosion product layers formed on mild steel in the Madrid atmosphere after 2 years (left) and 13 years (right) of exposure, and EDS spectrum for the latter.

Figure 9. Typical morphology of lepidocrocite (left) and goethite (right) formed in the atmospheres of El Escorial (rural) and Madrid (urban), respectively.

Figure 10. SEM/EDS results of corrosion layers formed on mild steel in skyward (left) and groundward (right) faces of the specimen after 13 years of exposure in the rural atmosphere of El Escorial.

Figure 11. SEM/EDS results obtained in a cross-section of the corrosion product layer formed on mild steel exposed in the industrial atmosphere of Bilbao.

Figure 12. SEM micrographs showing: a) goethite ("cotton balls") formations, lepidocrocite ("flowery" structures) crystals, and c) eroded surface due to the acid environment, in the industrial atmosphere of Bilbao.

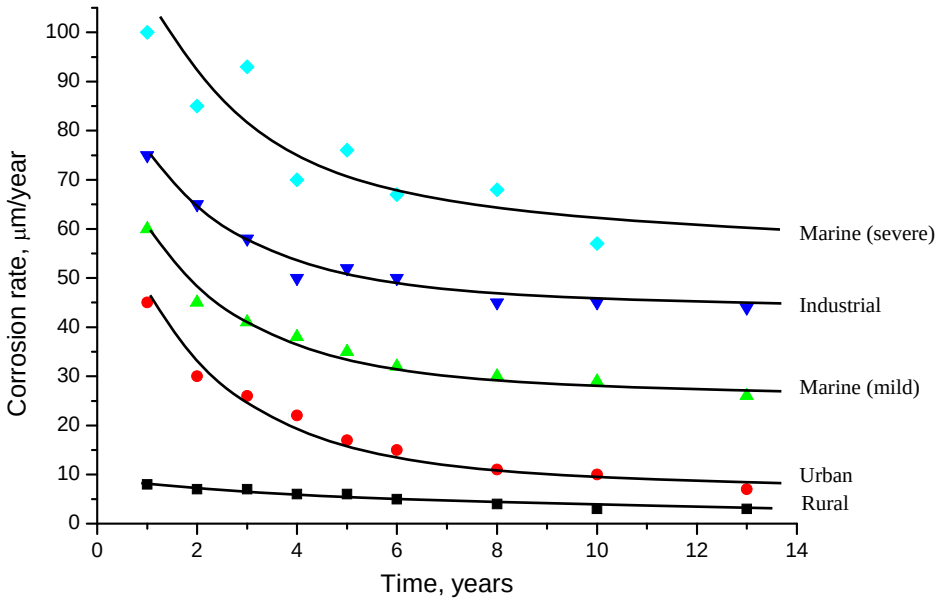
Corrosion rate, μm/year
Time, years
Marine (severe)
Industrial
Marine (mild)
Urban
Rural
0
10
20
30
40
50
60
70
80
90
100
0
2
4
6
8
10
12
14

Figure 1

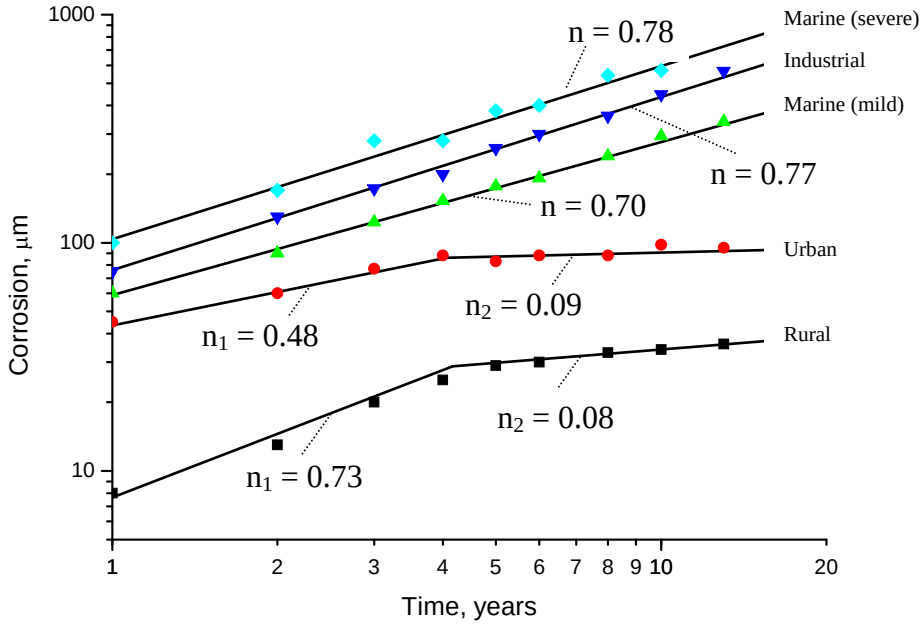
1000
100
10
Corrosion, μm
1
2
3
4
5
6
7
8
9
10
20
Time, years
n = 0.78
Marine (severe)
Industrial
Marine (mild)
n = 0.77
n = 0.70
Urban
n2 = 0.09
n1 = 0.48
Rural
n2 = 0.08
n1 = 0.73

Figure 2

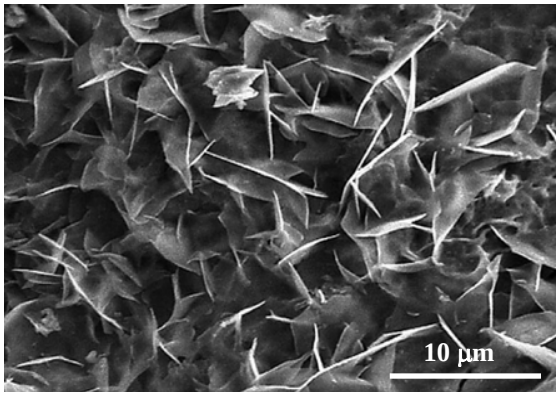

a)

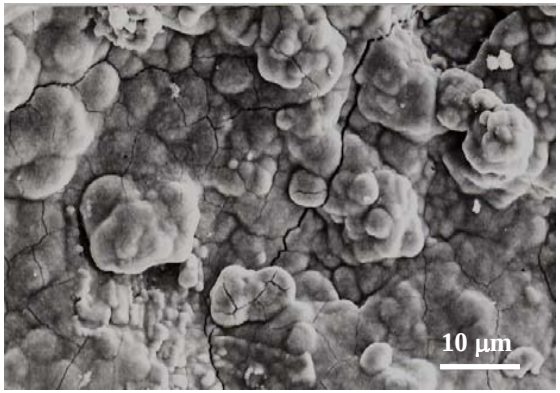

b)

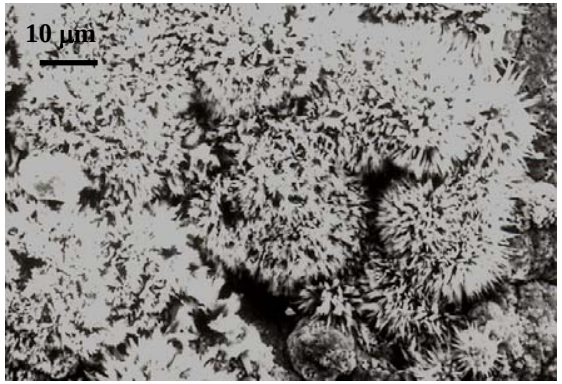

c)

Figure 3

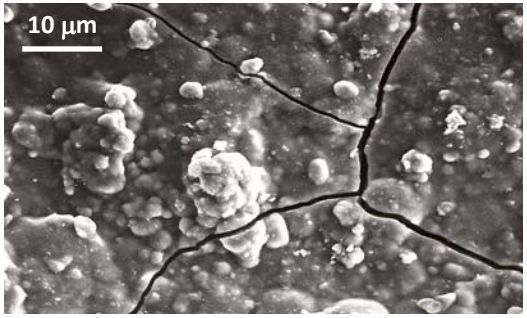

a)

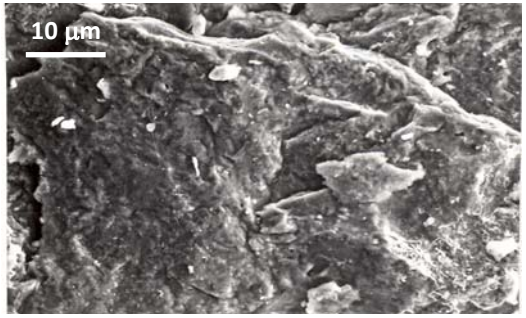

b)

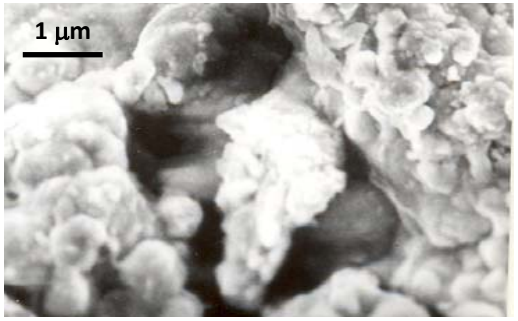

c)

Figure 4

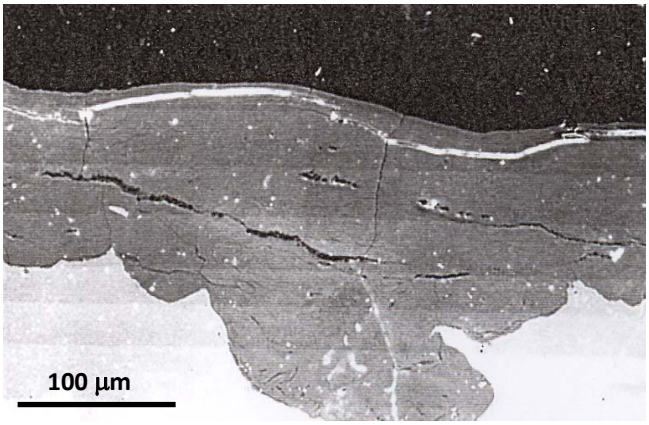

Figure 5

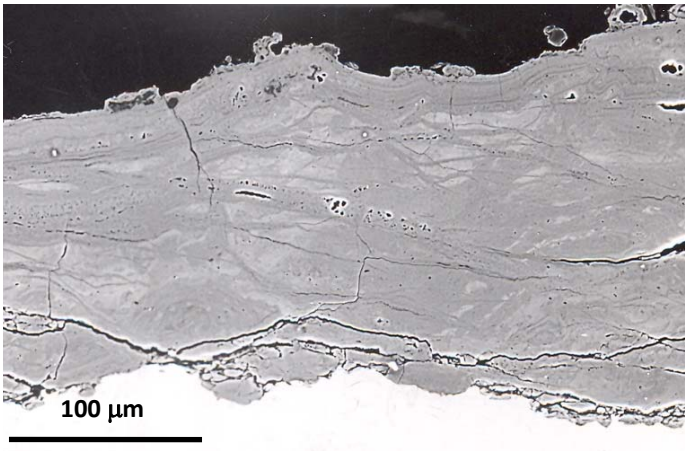

Figure 6

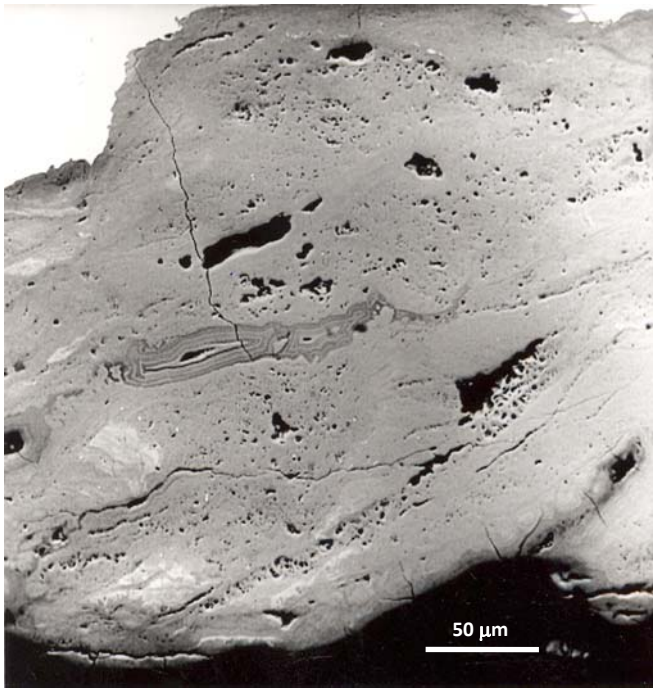

Figure 7

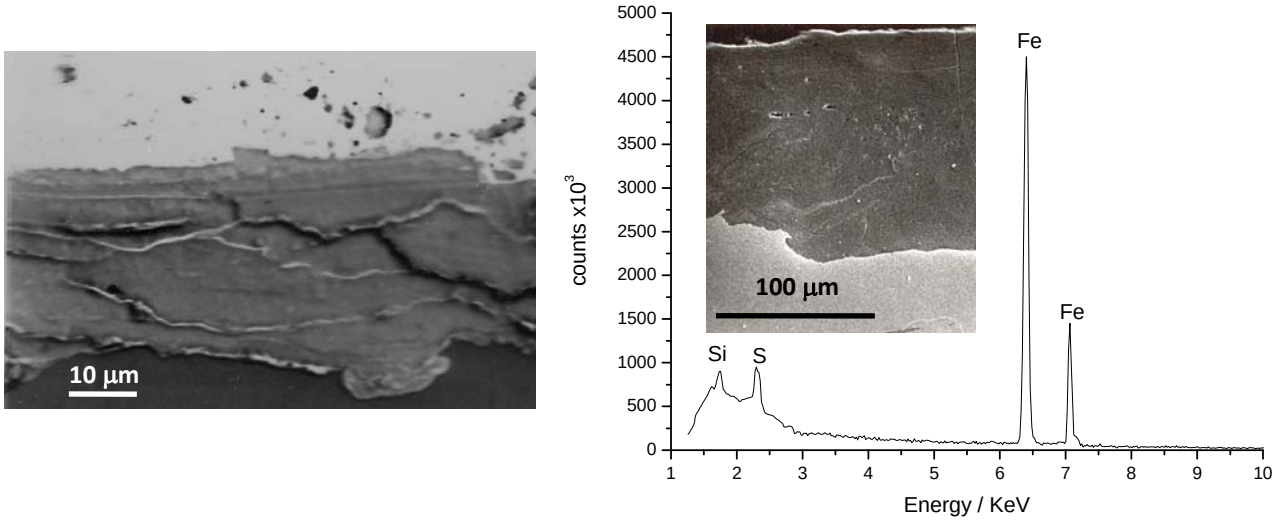
10 µm
100 µm
Si
S
Fe
Fe
counts x10^3
Energy / KeV
0
500
1000
1500
2000
2500
3000
3500
4000
4500
5000
1
2
3
4
5
6
7
8
9
10

Figure 8

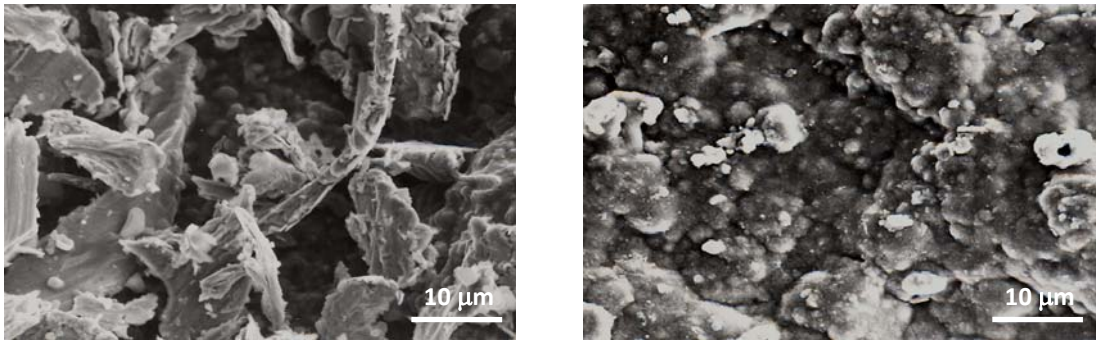

Figure 9

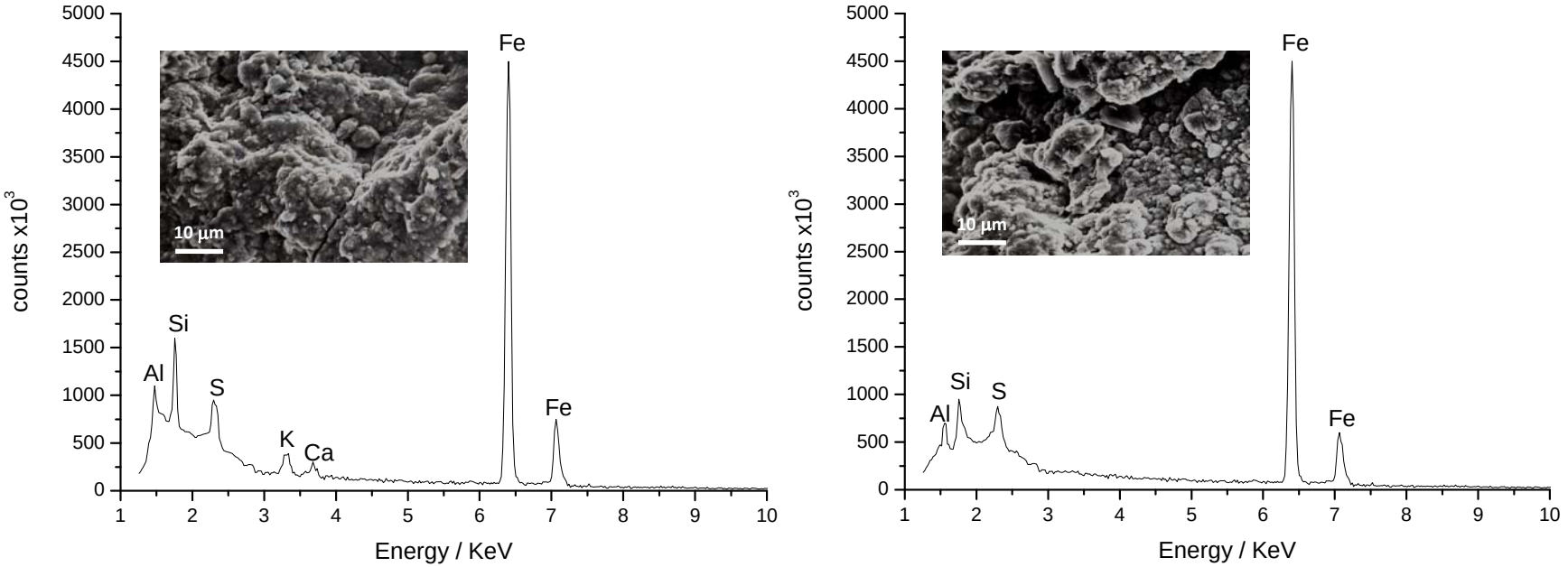

Figure 10

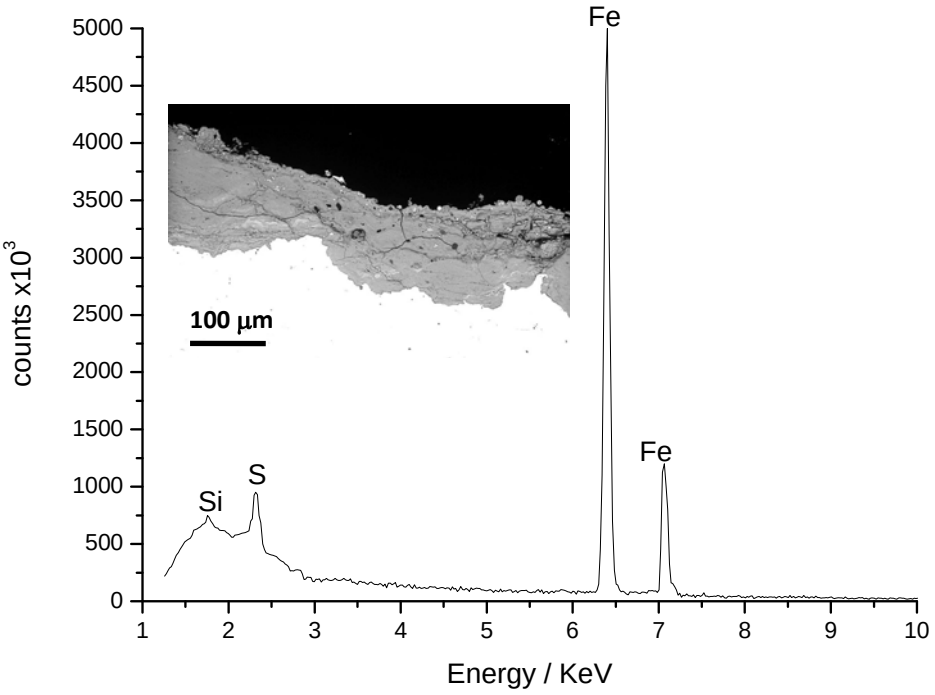
counts x10^3
5000
4500
4000
3500
3000
2500
2000
1500
1000
500
0
1
2
3
4
5
6
7
8
9
10
Energy / KeV
Fe
Fe
S
Si
100 μm

Figure 11

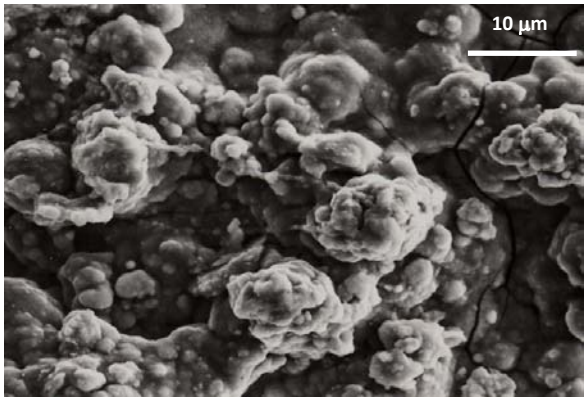

a)

b)

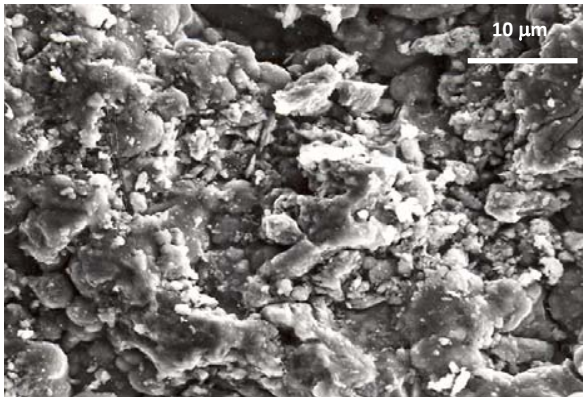

c)

Figure 12

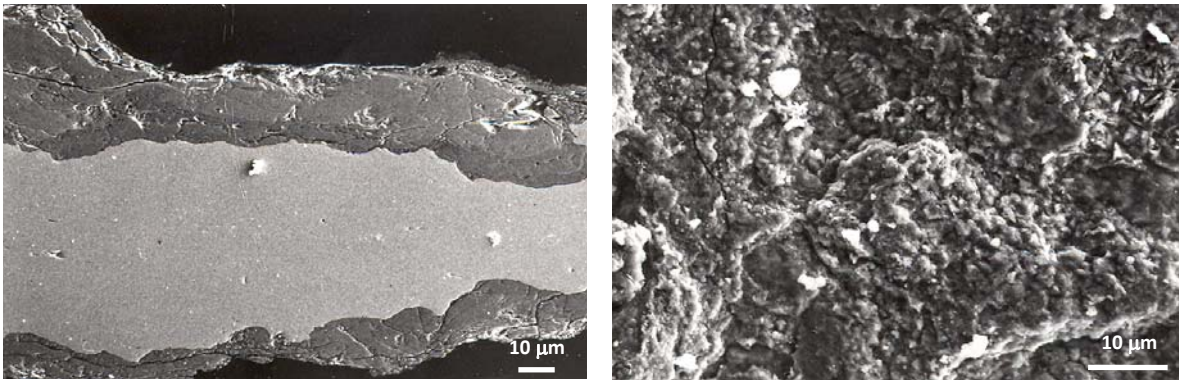

Figure 13

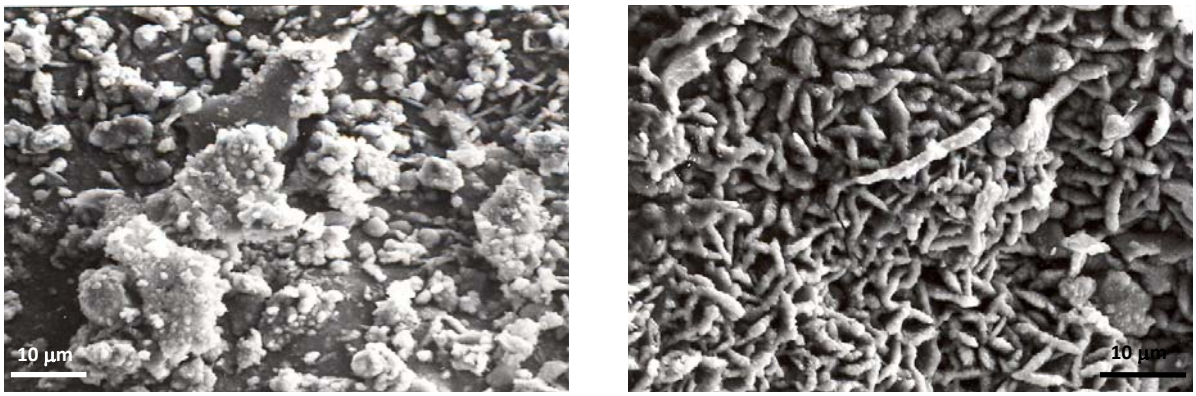

Figure 14

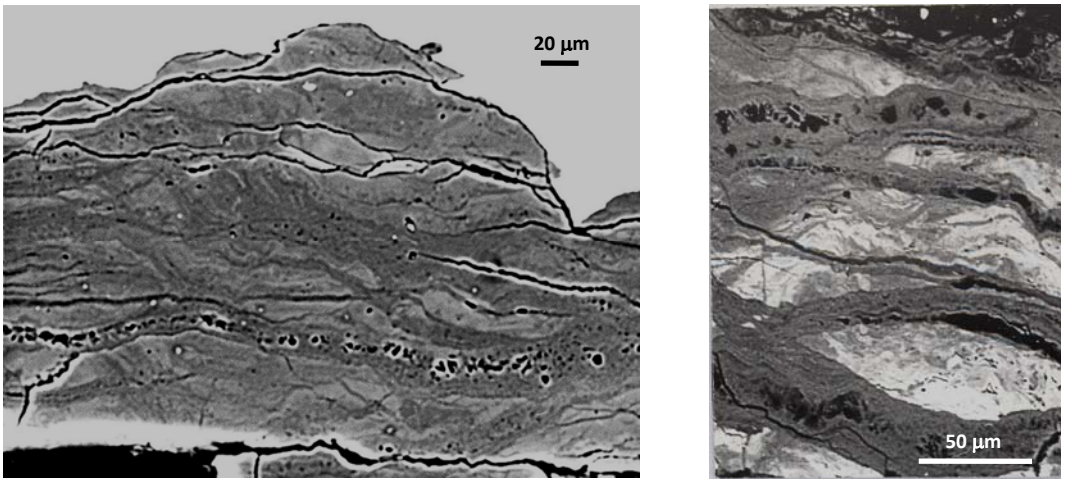

Figure 15

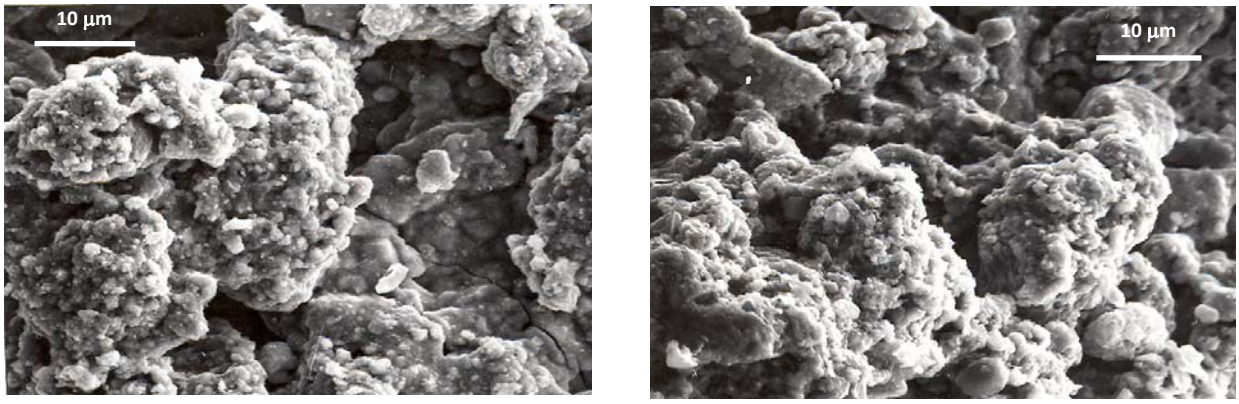

Figure 16

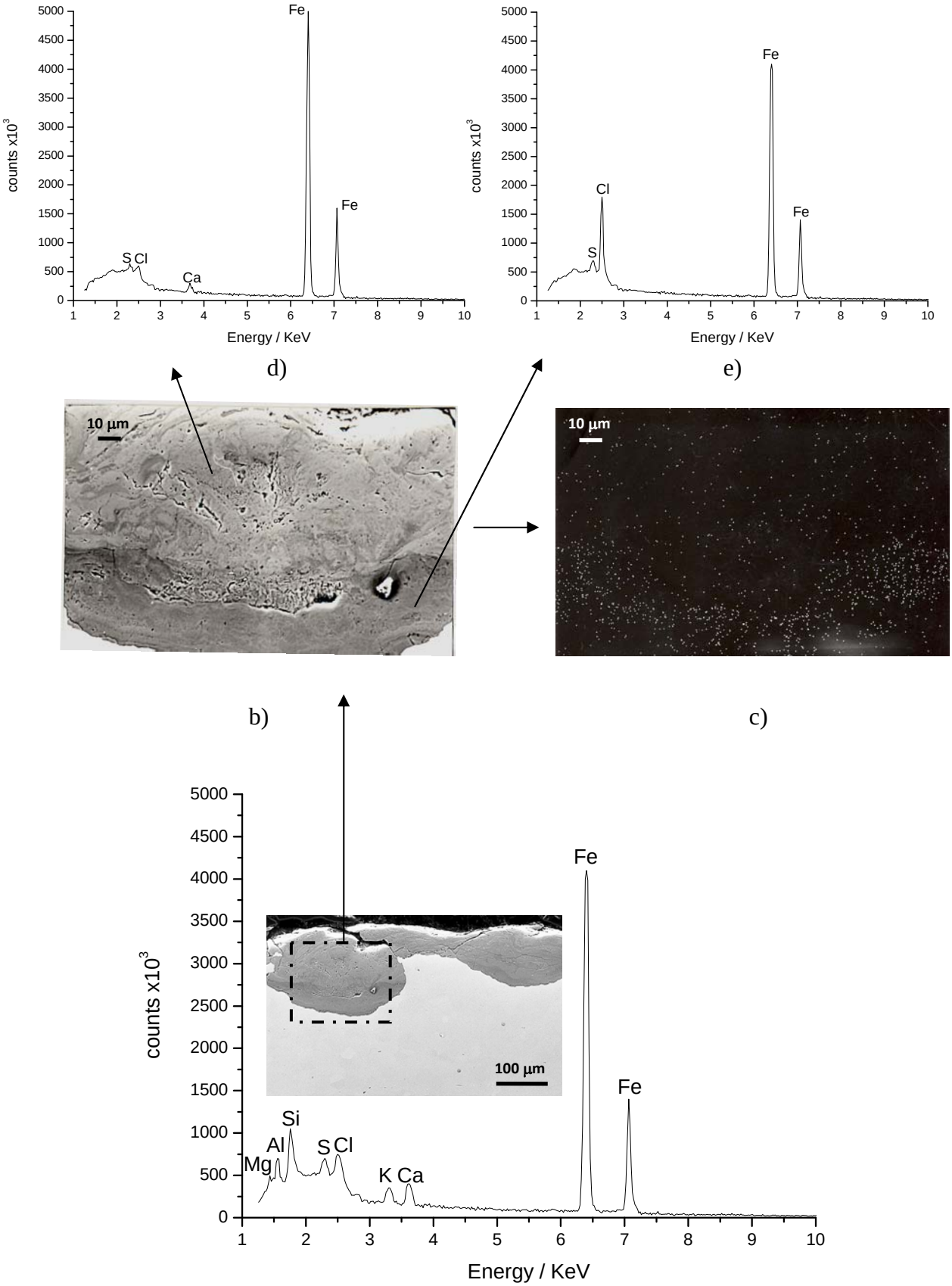
Fe
Fe
S Cl
Ca
counts x10^3
Energy / KeV
d)
Fe
Cl
S
Fe
counts x10^3
Energy / KeV
e)
10 µm
10 µm
b)
c)
Fe
Fe
Si
Al
S Cl
Mg
K Ca
100 µm
counts x10^3
Energy / KeV
a)

Figure 17

Table 1. Atmospheric corrosion stations. Environmental characteristics and corrosivity [8].

Atmosphere	Test site	Time of wetness (h/year)	Deposition rate ($mg/m^2.d$)		Mild Steel	
			SO_2	Cl^-	First year corrosion (μm)	ISO [9], corrosivity category
Rural	El Escorial	3900	8	Negligible	7.5	C2
Urban	Madrid	2100	56	Negligible	43.7	C3
Industrial	Bilbao	3000	81	41	69.6	C4
Marine						
Light	Barcelona	3200	52	27	49.9	C4
Severe	Alicante	4300	126	219	92.6	C5

Table 2. Crystalline phases of corrosion products of mild steel formed in the different atmospheres

Atmosphere	Test site	γ-FeOOH (lepidocrocite)	α-FeOOH (goethite)	β-FeOOH (akaganeite)	Fe_3O_4/ γ-Fe_2O_3 (magnetite/ maghemite)	$Fe_5HO_8.4H_2O$ (ferrihydrite)	α-Fe_2O_3 (hematite)	Observations
Rural	El Escorial	60.6%	24.6%		14.8%			On specimen
Urban	Madrid	60.6%	24.6%		14.8%			On specimen
Industrial	Bilbao	46.5%	18.9%		11.4%		23.3%	On specimen
Marine (mild)	Barcelona	39.1%	15.8%	35.5%	9.6%	Without quantify		On specimen
Marine (severe)	Alicante	43.2%	17.5%	39.3%				On powder obtained from flakes

Table 3. Extractable soluble salts contents (in mg/m^2) from the layers (non adherent and adherent) of corrosion products

Atmosphere	Test site	Sulphates			Chlorides		
		Non adherent	Adherent	Total	Non adherent	Adherent	Total
Rural	El Escorial	228	334	562	61	661	722
Urban	Madrid	215	758	973	77	1040	1117
Industrial	Bilbao	238	1172	1410	222	535	757
Marine	Barcelona	230	973	1203	1594	642	2236

Table 4. Some of the chemical species found in rust layers

Name	Composition
Oxides	
Hematite	α-Fe_2O_3
Maghemite	γ-Fe_2O_3
Magnetite	Fe_3O_4
Ferrihydrite	$Fe_5HO_8.4H_2O$
Hydroxides	
Ferrous hydroxide	$Fe(OH)_2$
Ferric hydroxide	$Fe(OH)_3$
Goethite	α-FeOOH
Akaganeite	β-FeOOH
Lepidocrocite	γ-FeOOH
Feroxyhyte	δ-FeOOH
Others	
Ferrous chloride	$FeCl_2$
Ferric chloride	$FeCl_3$
Ferrous sulphate	$FeSO_4$
Ferric sulphate	$Fe_2(SO_4)_3$